Improved Detection Using Negative Elevation Angles for Mountaintop WSR-88Ds. Part II: Simulations of the Three Radars Covering Utah

VINCENT T. WOOD, RODGER A. BROWN, AND STEVEN V. VASILOFF*

National Severe Storms Laboratory, Norman, Oklahoma

(Manuscript received 2 July 2002, in final form 2 December 2002)

ABSTRACT

About one-third of the Weather Surveillance Radar-1988 Doppler (WSR-88D) radars located in the western third of the United States are on the tops of mountains. These mountaintop radars employ scanning strategies that were designed for flatland radars, with the lowest elevation angle being +0.5°. Consequently, the radar signals are sent well above the populace and terrain surrounding the radar. The inability to adequately detect low-altitude weather events results in missed warnings of severe weather and in underestimates of the amount and areal extent of precipitation. Mountaintop radars could be utilized much more effectively if the scanning strategies included negative elevation angles. The state of Utah has the disadvantage that all three of the WSR-88Ds used by the National Weather Service to monitor weather events in the state are located on the tops of mountains. To determine the extent to which negative elevation angles would improve the detection capabilities of these radars over Utah and portions of the adjacent states, a WSR-88D simulation model is used to compare the existing scanning strategies with those that incorporate negative elevation angles. As might be expected, the use of negative elevation angles enhances low- to midaltitude detection of weather events over a much larger area than is possible using the existing scanning strategies. For example, the area where the centers of the beams from the three radars currently are within 1 km of the ground encompasses only 2% of the area within 230 km of the radars. Using negative elevation angles, the areal coverage within 1 km of the ground increases to over 30%.

1. Introduction

In the western third of the United States, about one-third of the Weather Surveillance Radar-1988 Doppler (WSR-88D) radars are located on the tops of mountains. Since the lowest elevation angle currently used by all WSR-88Ds is +0.5° (Crum et al. 1993), mountaintop radars are not able to detect many of the low-altitude weather phenomena that affect the population in the surrounding regions. Additionally, the spacing between WSR-88Ds in the western third of the country is much greater than across the plains and the eastern United States, which exacerbates the detection problem (Maddox et al. 2002). Current National Weather Service (NWS) policy does not allow any WSR-88D to scan below +0.5°.

In the first paper of this series on mountaintop WSR-88Ds, Brown et al. (2002) showed that the detection of low-altitude phenomena could be greatly improved if the Missoula, Montana, WSR-88D were to employ negative elevation angles. For example, using the conventional lowest elevation angle of +0.5°, they found that the percentage of simulated surface rainfall measured at that angle over flat terrain 1.5 km below the Missoula radar decreased from 80% at the radar to 1% at a range of 220 km. On the other hand, the percentage of simulated surface rainfall measured at a lower elevation angle of −0.8° remained between 80% and 95% throughout the same 220-km distance.

A mountaintop radar using negative elevation angles produces a different panorama than the elevation angles currently used by WSR-88Ds. Rather than increasing in height with increasing range under normal atmospheric conditions, the height of the radar beam first decreases and then eventually increases with range, producing a large coverage area where the beam is close to the terrain. The use of negative elevation angles can enhance low- to midaltitude detection of weather events, leading to improved warnings to the public.

NWS forecasters who are responsible for issuing warnings for the state of Utah and portions of the adjacent states are at a disadvantage because all three WSR-88Ds covering the area are located on the tops of mountains. The Salt Lake City WSR-88D (KMTX), is located on the top of a mountain at the southern end of the Promontory Mountains that extend into Great Salt

* Additional affiliation: Western Region Headquarters, National Weather Service, Salt Lake City, Utah

Corresponding author address: Vincent T. Wood, National Severe Storms Laboratory, 1313 Halley Circle, Norman, OK 73069.
E-mail: Vincent.Wood@noaa.gov

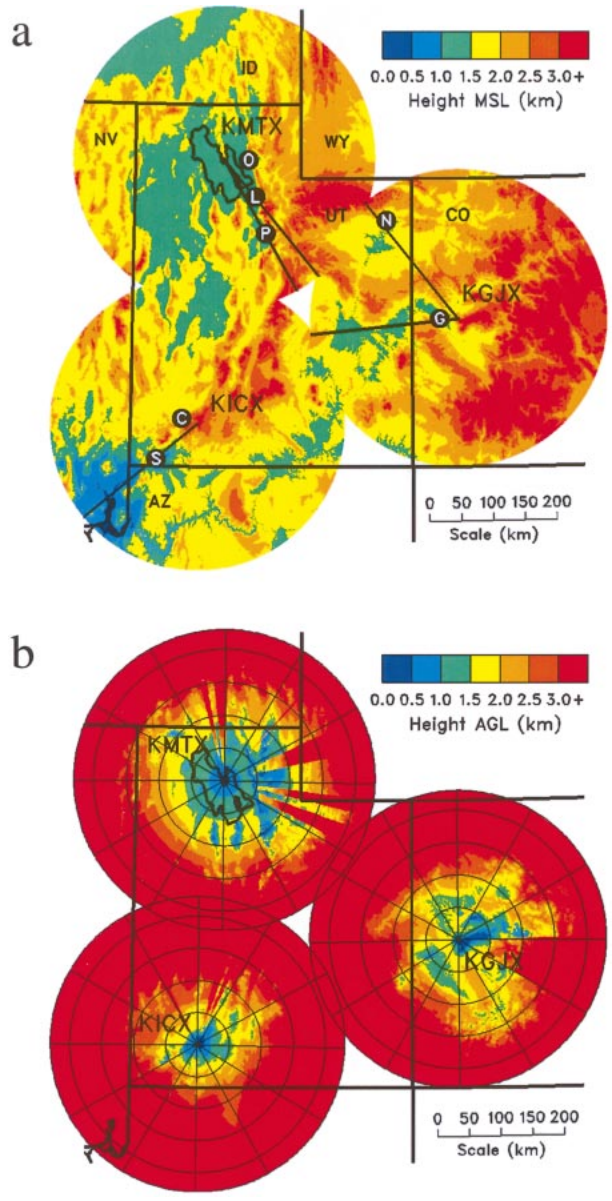

FIG. 1. (a) Terrain height above mean sea level (MSL) within 230 km of the KMTX, KGJX, and KICX WSR-88Ds. Black radial lines represent locations of vertical cross sections for conventional and mountaintop scanning strategies shown later in Figs. 6–10. Individual letters superimposed on black solid circles indicate the locations of cities mentioned in the text: C, Cedar City; G, Grand Junction; L, Salt Lake City; N, Naples, O, Ogden, P, Provo; and S, St. George. Polar coordinate terrain data courtesy of the WSR-88D Radar Operations Center. State boundaries and outline of Great Salt Lake are indicated by heavy lines. (b) Height above ground level (AGL) of lowest unblocked elevation angles of VCPs 11 and 21 within 230 km of simulated KMTX, KGJX, and KICX. Range circles are 50-km intervals; azimuth lines are at 30° intervals. State boundaries and outline of Great Salt Lake are indicated by heavy lines.

TABLE 1. Elevation angles for conventional VCPs 11 and 21 in comparison with simulated mountaintop VCPs for KMTX, KGJX, and KICX.

Scan No.	VCP 11	VCP 21	KMTX	KGJX	KICX
1	0.5°	0.5°	−0.4°	−0.9°	−0.9°
2	1.5°	1.5°	0.0°	−0.5°	−0.5°
3	2.4°	2.4°	0.4°	−0.1°	−0.1°
4	3.3°	3.3°	0.9°	0.4°	0.4°
5	4.3°	4.3°	1.5°	0.9°	0.9°
6	5.2°	6.0°	2.2°	1.4°	1.4°
7	6.2°	9.9°	3.0°	2.1°	2.1°
8	7.5°	14.6°	4.0°	3.0°	3.0°
9	8.7°	19.5°	5.3°	4.2°	4.2°
10	10.0°	—	6.9°	5.7°	5.7°
11	12.0°	—	9.0°	7.8°	7.8°
12	14.0°	—	11.6°	10.6°	10.6°
13	16.7°	—	15.1°	14.5°	14.5°
14	19.5°	—	19.5°	19.5°	19.5°

Lake about 75 km northwest of Salt Lake City. The Grand Junction WSR-88D (KGJX) is located about 30 km east of Grand Junction, Colorado, at the west end of the large, flat-topped Grand Mesa. The Cedar City WSR-88D (KICX), which is the highest radar site of all WSR-88Ds, is located atop a 3.2-km-high peak near Cedar City in southwestern Utah. The 230-km coverage area of each radar is shown in Fig. 1a.

The heights of the lowest unblocked beams of the current volume coverage patterns (VCPs) 11 and 21 (see Table 1 for specified elevation angles of those VCPs) above the terrain are presented in Fig. 1b. The dark and light blue shadings indicate the limited portions of the surrounding terrain that are within 1 km of the center of the lowest unblocked elevation angle. The red shading indicates that the lowest unblocked beam is more than 3 km above nearly all of the terrain beyond about 150 km of KMTX, 100–150 km of KGJX, and 100 km of KICX. The radial wedges in the figure indicate where the lowest elevation angle is blocked and a higher elevation angle represents the data that are closest to the ground beyond the range where blockage occurs. This type of display is referred to as a ''hybrid'' scan (Fulton et al. 1998). Hybrid scans can produce strange artifacts in precipitation estimates owing to the presence of data from several different elevation angles.

It is unfortunate that these radars are not being utilized to their full potential in detecting low-altitude weather phenomena and in estimating surface precipitation rates. This potential could be attained by using negative elevation angles. The objective of this paper is to estimate the extent to which negative elevation angles can improve the detection of low-altitude weather phenomena within the 230-km coverage areas of the three radars. The procedure for generating simulated volume coverage patterns for mountaintop radars is discussed in section 2. In sections 3–5, the advantages of using negative elevation angles with KMTX, KGJX, and KICX, respectively, are discussed. Section 6 describes the overall improvement in radar coverage over Utah and por-

tions of the adjacent states. Summary and conclusions are presented in section 7.

2. Simulation procedure

a. Scanning strategies for mountaintop radars

The procedure for producing a tailored set of elevation angles for a mountaintop radar has been discussed in detail by Brown et al. (2002). The most crucial part of the procedure is to determine the lowest elevation angle that adequately covers the surrounding terrain and population centers without encountering an undue amount of beam blocking by the terrain. Based on a theoretical study, Smith (1998) found that when the center of a radar beam is as close as about 0.3 beamwidth (about 0.3° for WSR-88Ds) above the ground, there is an acceptable balance between loss of power received from low-altitude features and the increase in ground return. We take advantage of these findings for determining the lowest elevation angle.

To begin, we estimate the distance that terrain features of interest—especially in the vicinity of population centers—are located below the altitude of the radar. Then, through an iterative process, we determine the negative elevation angle that just grazes a plane at the same distance below the radar. Computations were based on the following equation:

$$h = (r^2 + a_e^2 + 2ra_e \sin\phi)^{1/2} - a_e, \qquad (1)$$

where h is height of the radar beam relative to the radar, r is range from the radar site, a_e is effective earth radius that accounts for the standard index of refraction (using the WSR-88D value of 1.21 times the earth radius), and ϕ is elevation angle of the center of the radar beam (Doviak and Zrnić 1993). The lowest elevation angle then is defined as being 0.3° above the grazing angle.

To obtain a relationship between the height of a radar above the surrounding plane and the lowest elevation angle, the above process was repeated for a series of grazing elevation angles from 0.0° to −1.5° (to which 0.3° was added to obtain the lowest elevation angle). Then a polynomial was fitted to the lowest elevation angles as a function of the relative heights of the radar. The resulting polynomial expression is

$$\phi_1(\Delta z) = 0.3° - 0.922°\left(\frac{\Delta z}{z}\right)^{0.501}, \qquad (2)$$

where Δz is height of the radar above the surrounding terrain and z is a normalizing factor set equal to 1 km. The curve in Fig. 2 shows this relationship. None of the WSR-88Ds is more than 2 km above the surroundings and, therefore, there is no need for a radar to scan below −1.0° (Fig. 2). This is fortuitous because it is consistent with the extreme operating procedures for WSR-88Ds (National Weather Service 2000, 2–36). In order to prevent the antenna from hitting the platform, there is a mechanical stop at −4°. Then, to prevent the antenna from reaching the mechanical stop, there is an adjustable electrical stop around −1°.

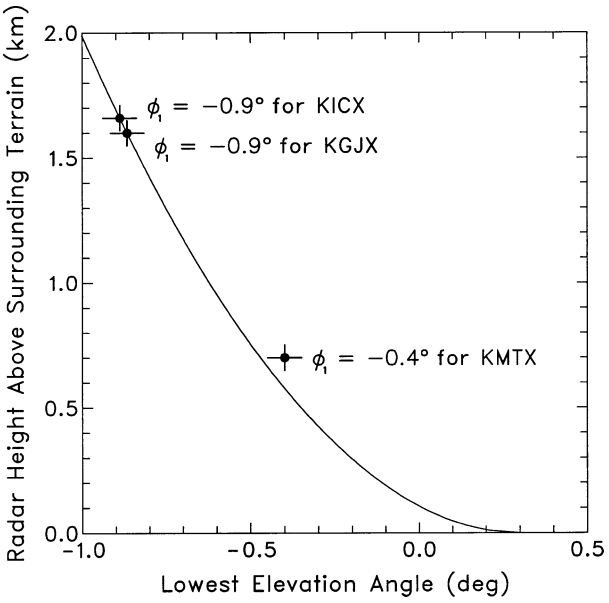

FIG. 2. Plot of calculated lowest elevation angles as a function of radar antenna heights above the surrounding terrain, based on Eq. (2).

The lowest elevation angles that were used in the simulations of KMTX, KGJX, and KICX are plotted in Fig. 2. The lowest angle for the Salt Lake City radar, KMTX, was raised 0.1° higher than indicated by the curve in order to clear some blocking terrain between the radar and the Salt Lake City area. With the highly variable terrain within the KICX coverage area (Fig. 1a), a minimum elevation angle of −0.9° was selected to adequately cover the surrounding terrain and to provide reasonable coverage over the lower terrain to the southwest of the radar. After determining the lowest elevation angle, the next step was to use the Brown et al. (2000) technique to compute a set of 14 elevation angles to produce adequate vertical resolution during a reasonable time interval (4–5 min). Table 1 lists the resulting elevation angles for the three simulated mountaintop radars. The lower elevation angles are separated by 0.4°–0.5°, instead of the current 1.0°, in order to produce better long-range detections.

Being in mountainous regions, one would anticipate that there will be some blockage of the radar beam at lower elevation angles. The procedure for computing the extent of beam blockage is described by Brown et al. (2002). If less than 60% of the beam is blocked, it is assumed that reflectivity values are usable with a correction beyond the range of partial blockage (e.g., Fulton et al. 1998). The beam beyond a given range at a given azimuth angle and elevation angle is assumed to be completely blocked when at least 60% of the beam is blocked. In this simulation, ground-clutter and sidelobe contaminations were not included.

b. Lowest unblocked elevation angles for the mountaintop VCPs

Using the mountaintop VCPs specified in Table 1, Fig. 3 shows the coverage areas of the lowest unblocked elevation angles for the KMTX, KGJX, and KICX radars. The lowest angle of −0.4° (dark blue area) within 230 km of the KMTX radar (Fig. 3a) is unblocked over nearly one-third of the area, including the major cities along the west side of the Wasatch Range (represented by Ogden, Salt Lake City, and Provo in Fig. 1a). The Wasatch Range blocks the lower elevation angles from northeast to southeast of the radar. The light blue area indicates that the next elevation angle of 0.0° covers essentially all of the area from south-southwest through north-northwest of the radar. The addition of the next elevation angle (0.4°) increases the unblocked coverage (green) to about 85% of the area. This angle is close to the lowest elevation angle of 0.5° that the KMTX WSR-88D currently uses. With the increased elevation angles (yellow and orange), the radar beam clears all of the terrain obstacles. The significant blockage to the north of the radar is caused by higher peaks in the Promontory Mountains just north of the radar.

With KGJX being 1.6 km above the Grand Valley in western Colorado, the curve in Fig. 2 indicates that the lowest elevation angle should be −0.9°. The lowest unblocked elevation angles for the various portions of the KGJX radar coverage area are presented in Fig. 3b. The small dark blue area shows that the lowest elevation angle (−0.9°) covers Grand Valley (extending to the west-northwest of the radar) and Interstate 70, which runs westward into Utah, as well as other populated areas within 50–100 km of the radar. More than one-half of the coverage area within 230 km has an unobstructed beam with the next elevation angle (light blue indicating −0.5°). With the addition of the −0.1° elevation angle (green), three-quarters of the coverage area is unobstructed. The blockage (yellow and orange) east-northeast through south-southeast is caused by the portion of Grand Mesa that extends to the east-southeast of the radar.

The terrain within the coverage area of KICX also is highly variable, ranging from 3 km MSL near the radar to 0.5 km MSL in the Lake Mead area of southeast Nevada (Fig. 1a). Figure 3c shows the lowest unblocked elevation angles for the coverage area within 230 km of the KICX radar. The lowest elevation angle of −0.9° (indicated by the dark blue areas) is unblocked for over one-half of the area. With the addition of the next elevation angle (−0.5°), about 85% of the coverage area is unblocked. The yellow-to-dark-orange sector indicates terrain blockage at higher elevation angles owing to higher peaks just north-northeast of the radar. The narrow red sector represents blockage caused by a nearby tower.

c. Practical considerations

Potential radar operational problems such as radar beam sidelobes, ground clutter, and nonstandard conditions for the index of refraction are anticipated, but are not addressed in this study. With the increased amount of terrain blockage at the lower elevation angles, the suppression of sidelobes may be a challenge. Interstate or train traffic currently are detected in the sidelobes of the lower elevations with the conventional VCPs and cause false triggering of the algorithm designed to detect tornadoes. Nonstandard conditions for the index of refraction (e.g., Battan 1973) may be another challenge for forecasters. The conditions exist when low-altitude situations, such as nocturnal radiational cooling and post-cold-frontal passage, occur in the valleys. In these situations, the resulting temperature inversion leads to anomalous propagation, where any radar beam entering the inversion layer bends downward and intercepts the ground.

The prospect of using negative elevation angles raises the question as to whether there will be increased risks to nearby people when the transmitted energy is directed more toward the ground (e.g., Brown et al. 2002). An exhaustive study of potential hazards was made for an environmental impact statement prepared prior to the installation of the WSR-88Ds (SRI International 1993). The study found that energy transmitted by the rotating WSR-88D antenna was only 1%–2% of the conservative safety level in effect at the time of the study, even if the radar were scanning directly past a person outside the radar enclosure. The transmitted energy rapidly decreases in magnitude with increasing distance from the radar. Therefore, lowering the antenna by 1.0°–1.5° does not pose a threat to those people who may be in the immediate vicinity of a remote mountaintop radar.

3. Salt Lake City radar (KMTX)

The Salt Lake City WSR-88D, KMTX, is located 2.0 km MSL on a mountain at the south end of the Promontory Mountains that extend into Great Salt Lake about 75 km northwest of Salt Lake City (L in Fig. 1a). The largest cities in Utah are nestled up against the western side of the Wasatch Range from Ogden (O in Fig. 1a), about 35 km east of the radar, to Provo (P in Fig. 1a) located about 130 km to the south-southeast. Most of these population centers and the surface of Great Salt Lake lie about 0.7 km below the radar (Dunn and Vasiloff 2001).

a. Forecasting and warning challenges for the KMTX coverage area

The lack of detection of low-altitude weather phenomena owing to the elevated scanning of the KMTX radar presents several major challenges to forecasters at the Salt Lake City NWS Weather Forecast Office (WFO). The issuance of a severe storm warning depends in part on a careful evaluation of the characteristics and evolution of reflectivity and Doppler velocity signatures in the lower parts of the storm. Since most of the con-

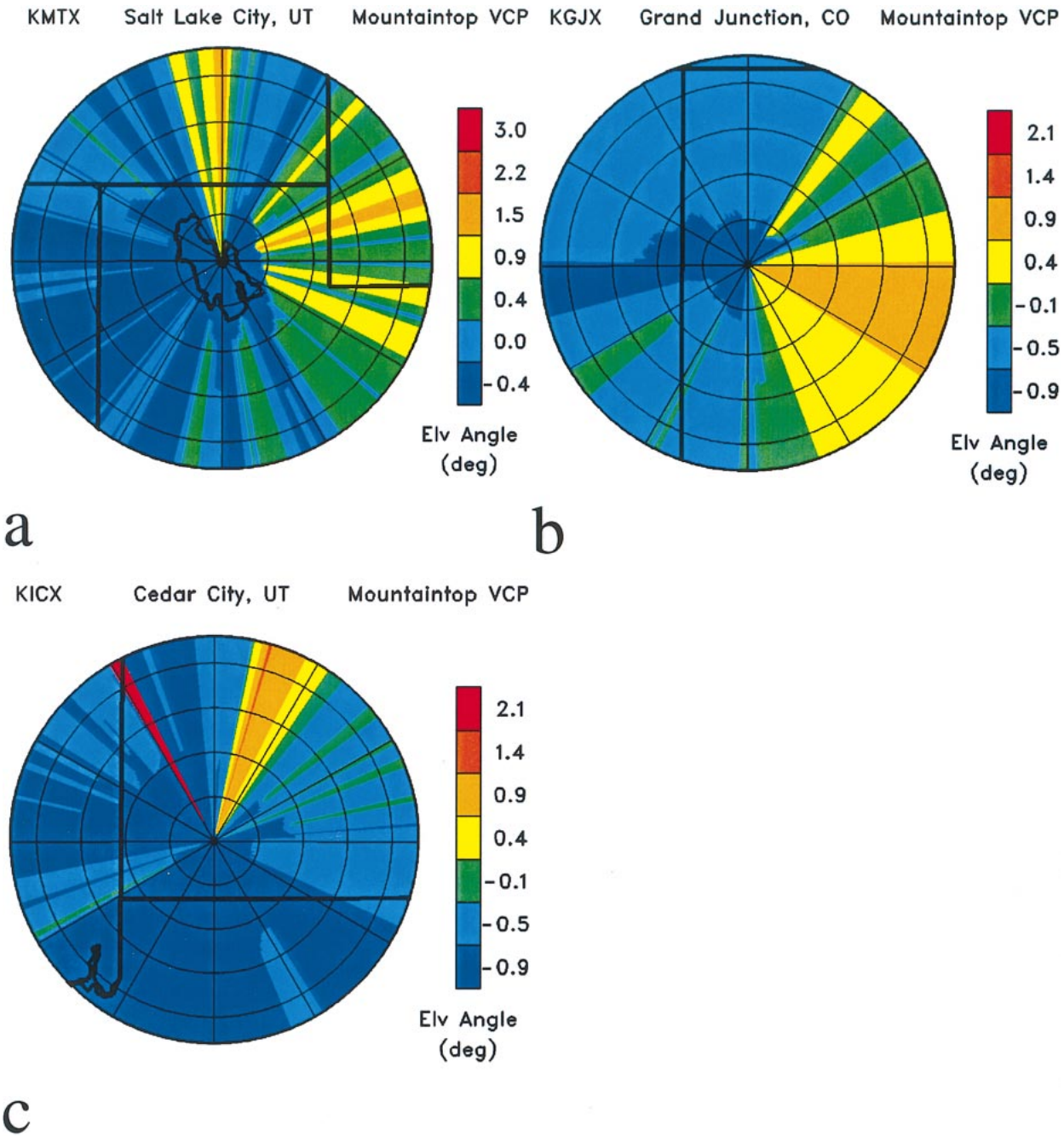

FIG. 3. Plot of lowest unblocked simulated elevation angles within 230 km of (a) KMTX, (b) KGJX, and (c) KICX. Unblocked elevation angles are indicated by coded colors on the right side of each panel. Range circles are 50-km intervals and azimuth lines are separated by 30° intervals. State boundaries are indicated by heavy lines.

vective severe weather in northern Utah comes from low-topped supercells, forecasters are hampered by the lack of observations at crucial levels with the storms.

Low-altitude boundaries play an important role in the forecasting process and they are rarely seen on the KMTX radar displays. The passages of storm outflow boundaries and of lake-breeze fronts off Great Salt Lake have an impact on flight operations at Salt Lake City International Airport. These boundaries, and especially the collision of the boundaries, represent the convergence zones along which storms can be initiated (e.g., Wilson and Schreiber 1986; Wilson and Mueller 1993). If forecasters were able to detect the existence and movement of these boundaries, they could better anticipate the timing and location of some thunderstorm development. In fact, owing to the lack of negative ele-

vation angles, the climatologically rare F2 tornado of 11 August 1999 formed along a lake-breeze front that was ill-defined on KMTX (e.g., Dunn and Vasiloff 2001; Vasiloff 2001).

In regions of the country, like the western states, where the subcloud environment typically is dry, it is important to distinguish between rain reaching the ground and rain that evaporates before reaching the ground. Whether rain reaches the ground has a great impact on quantitative precipitation estimates (QPEs) and consequently has a great impact on whether flash flooding will occur (e.g., Davis and Jendrowski 1996). The new Flash Flood Monitoring and Prediction (FFMP) capability at NWS offices depends on having accurate QPEs (e.g., Filiaggi et al. 2002). Using the current WSR-88D scanning strategies, there is only a small area in the immediate vicinity of KMTX where the radar beam is low enough to detect precipitation within 1 km of the surface.

During the winter, shallow snowstorms and especially lake-effect snows pose a forecasting problem (e.g., Carpenter 1993; Steenburgh et al. 2000). The radar frequently overshoots the snowstorms that are only a few kilometers deep, especially at distances greater than 100–150 km from the radar. Consequently, there are large areas within the radar coverage region where the forecaster does not know whether it is snowing. Where there are indications of snow, snowfall intensity cannot be estimated because the lowest radar beam is too high above the ground.

b. Detection improvements using negative elevation angles

As an initial investigation of the advantages of using the mountaintop VCP over current VCPs 11 and 21, we assume that the radar is located on an infinitesimally narrow mountain peak 0.7 km above a flat plane. Figure 4a shows idealized vertical profiles of divergence, as might be found with a microburst, and convergence, as might be found with a gust front or lake-breeze front. The percentage of the surface divergence/convergence measured at the lowest elevation angle is shown in Fig. 4b. Using current VCPs 11 and 21, about 75% of surface divergence/convergence is measured near the radar and it decreases to zero at about 60 km and beyond where the beam overshoots the phenomenon. In contrast, when the mountaintop VCP is used, the percentage of measured surface divergence/convergence increases from 75% near the radar to nearly 85% at a distance of 50–60 km. At a distance of about 140 km, 50% is still detectable. For a given percentage of detection, the increase in the range of detection for the mountaintop VCP relative to VCP 11 is over 100 km.

For a second example, we simulated a widespread snowstorm occurring over the flat plane based on actual KMTX measurements (Fig. 5). A vertical profile of modeled reflectivity in snow is assumed to decrease

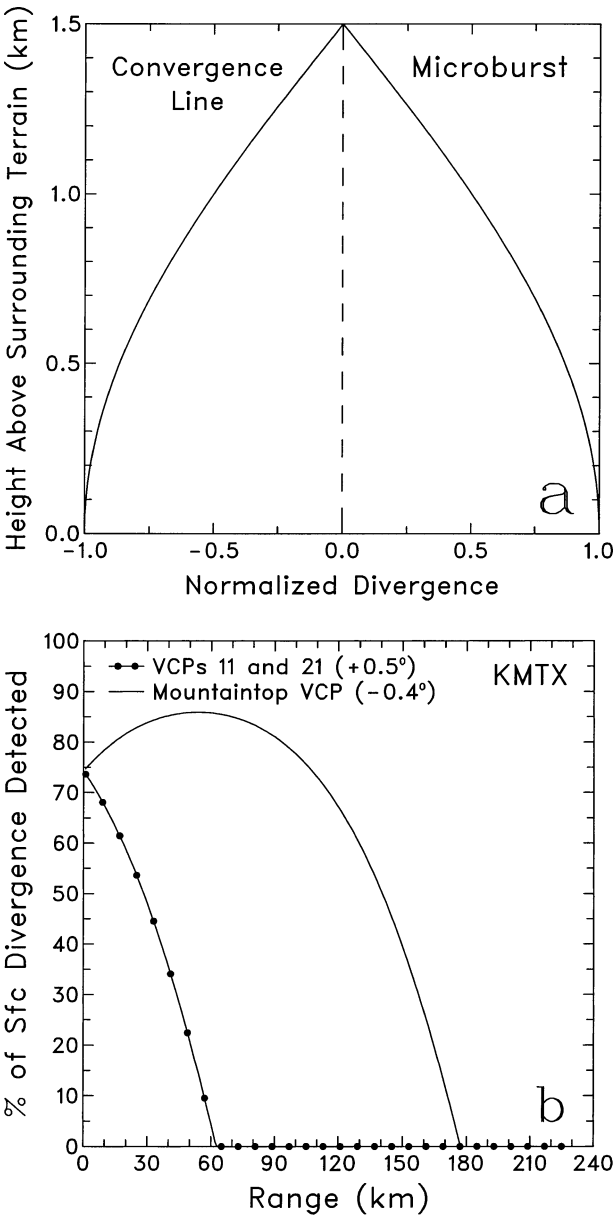

FIG. 4. Simulated low-altitude divergence for KMTX. (a) Divergence profiles as a function of height (normalized by surface values) for a convergence line and a microburst. (b) Percentage of the surface divergence detected at the lowest elevation angle for VCPs 11 and 21 (dotted curve) and the mountaintop VCP (solid curve). The radar is assumed to be 0.7 km above a plane surface representing the terrain surrounding KMTX.

linearly from 30 dBZ at the surface to 10 dBZ at 4 km. A sinusoidal variation simulating cellular features perturbed the profile as a function of range and then random noise was added to the perturbations before the vertical cross section was sampled by the simulated radar. Near the radar, low-altitude detections using VCP 11 provide a fair representation of snowfall occurring at the surface (Fig. 5a). However, since the height of the radar beam increases with range under normal atmospheric condi-

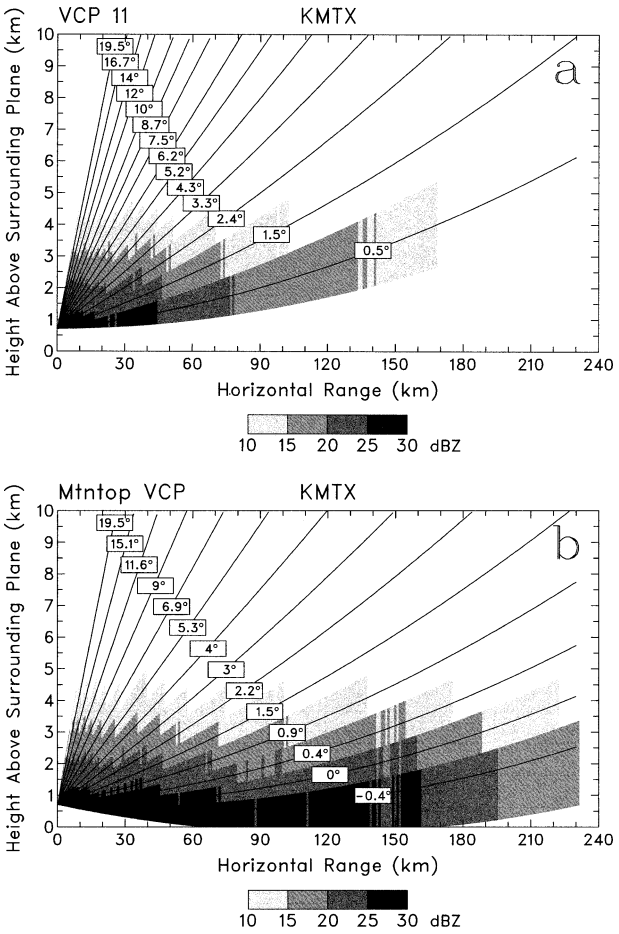

FIG. 5. Simulated detection of a modeled widespread snowstorm using (a) VCP 11 and (b) the mountaintop VCP with KMTX. The vertical depth of a displayed reflectivity value extends halfway to the adjacent elevation angles; for the highest and lowest elevation angles, the side without an adjacent elevation angle extends one-half beamwidth.

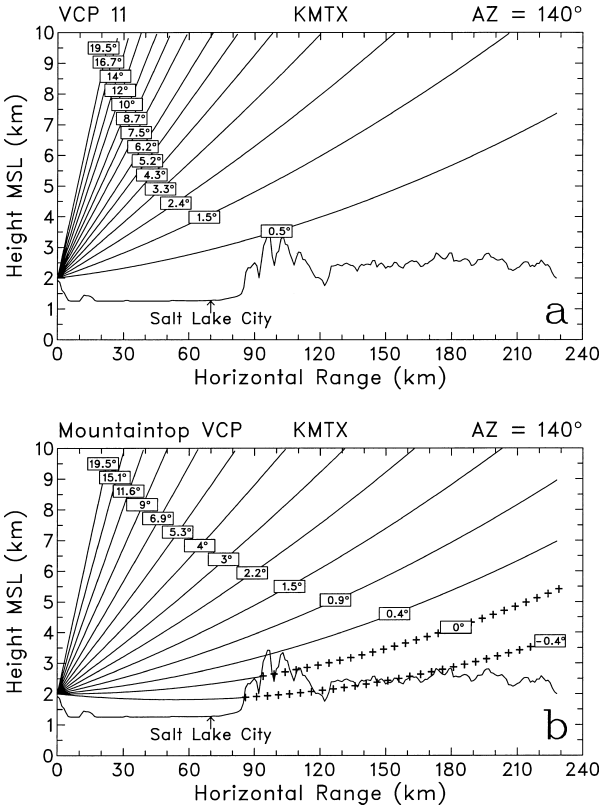

FIG. 6. Vertical cross section of (a) conventional scanning strategy VCP 11 and (b) simulated mountaintop VCP for KMTX along 140° azimuth over Salt Lake City. The curves represent beams with no or partial blockage (less than 60%). In (b), plus signs represent total beam blockage (greater than 60%).

tions, the center of the lowest radar beam is within 1 km of the ground only within 30 km of the radar. With increasing range, only higher portions of the snowstorm are detected. Beyond about 165 km, there is no radar indication that snow is occurring at those ranges. On the other hand, using negative elevation angles, the beam descends toward the ground before it eventually starts curving upward. Not only does the mountaintop VCP in Fig. 5b indicate that it is snowing at least to 230 km, but the center of the lowest radar beam is within 1 km of the ground out to a range of 140 km. Here again, the increase in the range of detection for the mountaintop VCP is over 100 km.

Using actual terrain data instead of a flat plane, vertical cross sections were prepared to compare the current VCP 11 and the mountaintop VCP over Salt Lake City and Provo; these cross sections shown in Figs. 6 and 7, respectively, are indicated by black lines radiating from KMTX in Fig. 1a. In the Salt Lake City area (Figs. 6a and 6b), the center of the lowest beam for the mountaintop VCP is 0.5–0.6 km above the ground, whereas the lowest beam for VCP 11 is at a height of 1.5–1.8 km. The two lowest elevation angles of the mountaintop VCP that provide the enhanced coverage over the city are blocked by the Wasatch Range farther to the southeast.

In the Provo area (Figs. 7a and 7b), about 130 km south-southeast of the radar, the lowest elevation angle of VCP 11 is about 3 km above the terrain. Using the mountaintop VCP, the lowest elevation angle is less than 1 km above the terrain. In fact, at the azimuth of 150°, the lowest mountaintop VCP elevation angle essentially parallels the terrain. The more closely spaced lower elevation angles of the mountaintop VCP clearly produce a dramatic improvement in the vertical resolution of low-altitude weather phenomena.

4. Grand Junction radar (KGJX)

The Grand Junction, Colorado (KGJX), WSR-88D is located about 30 km east of Grand Junction (G in Fig. 1a) at the west end of Grand Mesa, one of the largest flat-topped mountains in the world. The radar is at a

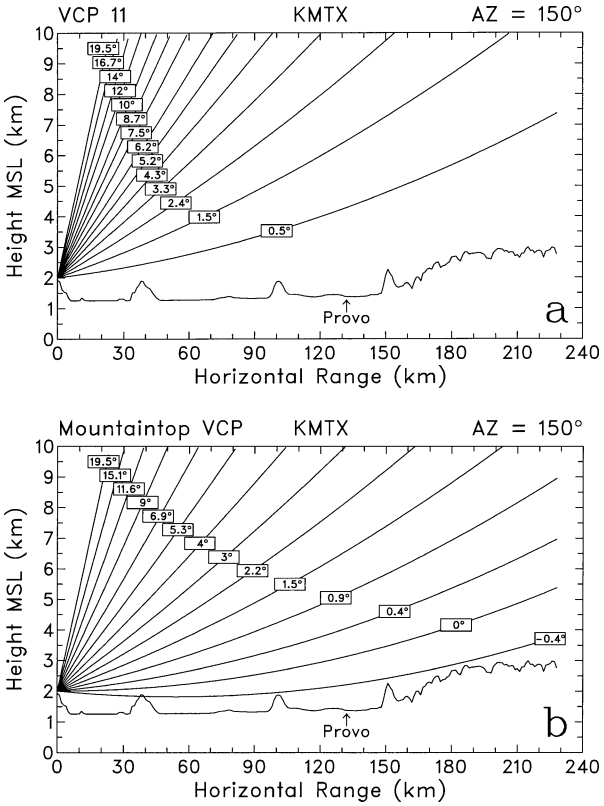

FIG. 7. Same as in Fig. 6 except along azimuth 150° over Provo, UT.

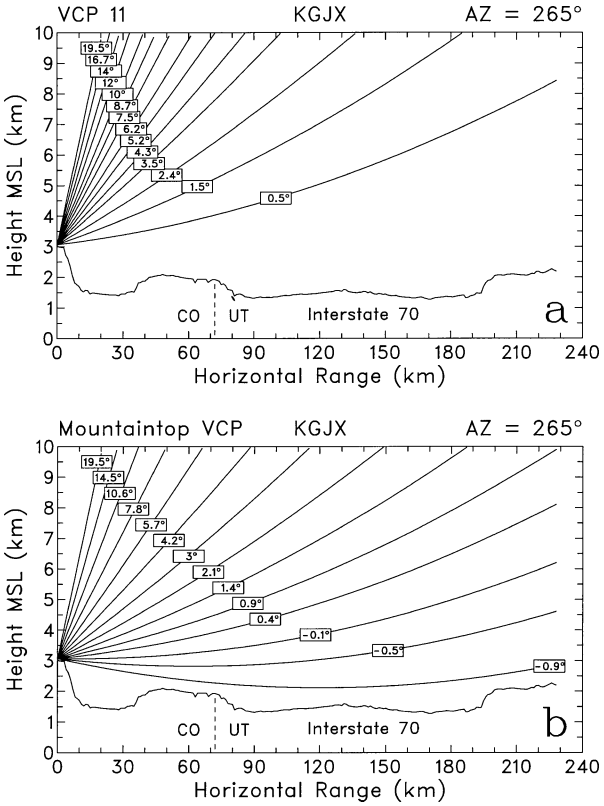

FIG. 8. Same as in Fig. 6 except for KGJX along azimuth 265° over Interstate 70.

height of 3 km MSL, which places it about 1.6 km above Grand Valley, which extends to the northwest of Grand Junction. The main artery of transportation through west-central Colorado and east-central Utah is Interstate 70, which passes through Grand Valley and then turns westerly as it traverses eastern Utah. The black line extending to the west from the radar in Fig. 1a is a straight-line approximation to the location of Interstate 70 within the KGJX coverage area.

a. Forecasting and warning challenges for the KGJX coverage area

The forecasting problems associated with KGJX are similar to those with KMTX. A significant problem is the failure to detect shallow precipitation events, primarily in the outer portions of the WFO's warning area, which includes nearly all of Colorado west of the Continental Divide and the eastern fifth of Utah. During the summer, much of the rainfall comes from relatively shallow monsoonal thunderstorms. With the lowest angle from the current VCPs being +0.5°, it is difficult to detect these storms, especially those over the national parks of southeast Utah where hikers can be caught unawares by deadly flash floods.

During the winter, the detection capability is even worse with snowstorms being much shallower than summertime rainstorms. With Interstate 70 being the main transportation route through the region, forecasters at the Grand Junction forecast office are unable to monitor low-altitude snowfall conditions along the route using current VCPs.

b. Detection improvements using negative elevation angles

Vertical cross sections of VCP 11 and the simulated mountaintop VCP along the Interstate 70 corridor are presented in Fig. 8. It is abundantly clear in Fig. 8a that the current VCPs available for KGJX do not provide adequate information. In contrast to VCP 11, Fig. 8b shows two significant advantages of the simulated mountaintop VCP. The height of the lowest negative elevation angle decreases and then increases with range, keeping the beam within 1 km of the ground throughout most of the coverage area. Second, the closer spacings between the lower elevation angles produce an improvement in resolving vertical characteristics of low-altitude phenomena, especially at long ranges.

On 3 September 1999, a rare tornado- and hail-producing minisupercell occurred in the northwest corner of the Grand Junction warning area (Colton et al. 2000). An F1 tornado did considerable damage in portions of Naples, which is located in the northern part of the Uinta

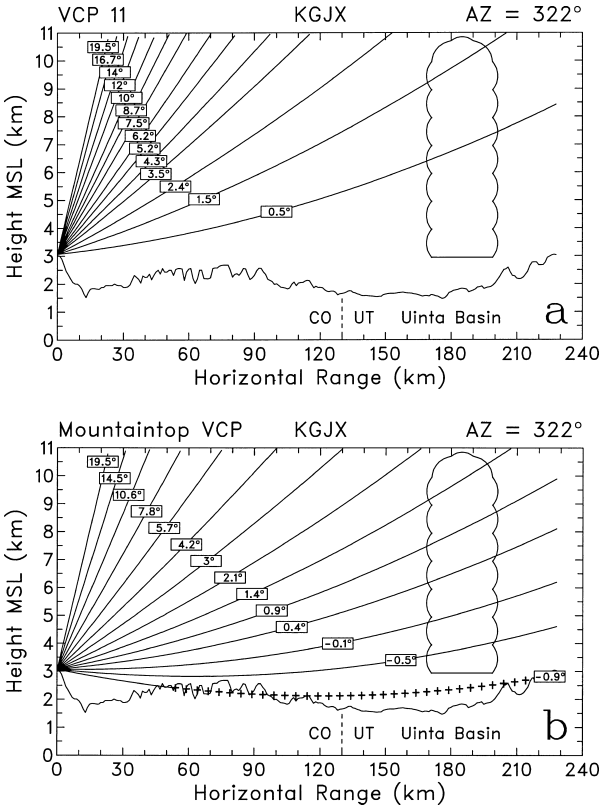

FIG. 9. Same as in Fig. 6 but for KGJX along azimuth 322° over Naples, UT, in the Uinta Basin. A schematic thunderstorm is shown.

Basin of northeast Utah; the Uinta Basin is the large depression shown in Fig. 1a near N to the northwest of KGJX. The schematic cloud and simulated elevation angles in Fig. 9a illustrate the type of radar coverage that the forecasters had available at the time of the tornado. The figure shows that the 0.5° elevation angle provided forecasters with minimal information about the midlevels of the storm, and no information about the lower parts of the storm. Doppler velocity measurements at 1.5° indicated the presence of divergence near storm top. The lack of vertical resolution prevented forecasters from diagnosing the depth of rotation in the storm. Colton et al. (2000) conclude that there is a need for ''alternative VCPs which will allow for lower slices.''

An example of how lower slices would permit forecasters to better resolve and monitor this type of storm is shown in Fig. 9b. In spite of the fact that the lowest elevation angle is blocked by terrain, the lower elevation angles are separated by about one-half beamwidth instead of 1° so there would still be measurements in the lower part of the storm. In fact, the smaller interval between elevation angles provides much greater vertical resolution of processes taking place throughout the storm. One might argue that overlapping the beamwidth every half-beamwidth does not provide more ''independent'' information than the elevation angles in VCP 11. The point is that, even though storm characteristics are smeared over the vertical depth of the beam (about 3 km for the Naples storm), the vertical variation of the smeared values with the mountaintop VCP provides more information than provided by smeared values at only 0.5° and 1.5°.

5. Cedar City radar (KICX)

The Cedar City WSR-88D (KICX) is located on top of Blow Hard Mountain (3.2 km MSL) in southwestern Utah (Fig. 1a). The radar is about 20 km east-southeast of Cedar City, which is at an elevation of 1.8 km MSL in the valley at the base of the mountain range. The terrain to the southwest of the radar drops off quickly to about 0.7 km MSL in the vicinity of St. George (S in Fig. 1a), just north of the Arizona border. Beyond, there is a more gradual descent to Lake Mead (0.5 km MSL) at the southeast tip of Nevada. Not being located near a forecast office, KICX is controlled remotely from the NWS WFO in Salt Lake City.

a. Forecasting and warning challenges for the KICX coverage area

A major challenge for forecasters at the Salt Lake City WFO arises from the inability to adequately detect or resolve precipitating systems in southern Utah owing to the elevated scanning of KICX. During the cool season, shallow rainstorms form as strong, moist southerly flow is lifted by the rising terrain. These storms have the capability of producing heavy rainfall, but without proper radar detection, it is not known how much of the rain aloft is evaporating before it reaches the surface. This situation is especially serious in the Virgin River watershed, which drains the area immediately south and southwest of the radar, where the radar completely overshoots cool-season rainstorms that produce flooding by raining onto snow surfaces.

During the warm season, the national parks and recreation areas of southern Utah attract millions of tourists and hikers. There is almost no coverage over the Glen Canyon Recreation Area (east through southeast of the radar), where the passage of a cold frontal or storm outflow boundary can overturn boats or drive them aground (L. Dunn 2002, personal communication). Hikers in the canyons of the various national parks in the area are at the mercy of flash floods. If upstream storms are not detected because of the elevated scanning strategy, it is impossible for the WFO to issue flash flood warnings.

b. Detection improvements using negative elevation angles

An advantage of using negative elevation angles with KICX is illustrated in Fig. 10. The vertical cross sections are along the black line in Fig. 1a that radiates southwestward from the radar and passes over the city of St.

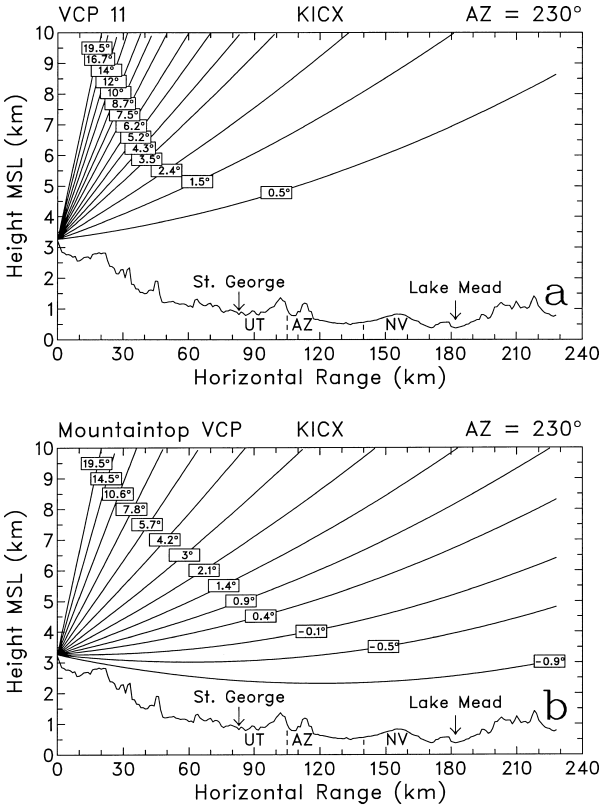

FIG. 10. Same as in Fig. 9 but for KICX along azimuth 230° over St. George, UT, and the Lake Mead area of southeast NV.

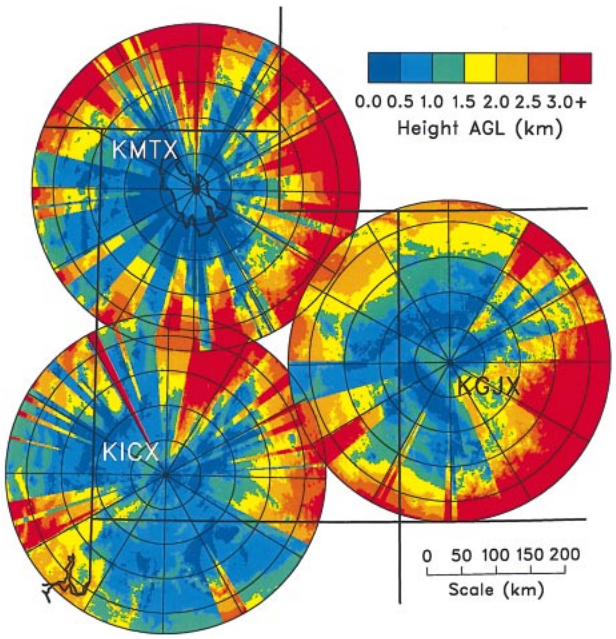

FIG. 11. Same as in Fig. 1b but for simulated mountaintop VCPs having negative elevation angles.

George and over terrain sloping downhill toward Lake Mead. Using conventional VCP 11 (Fig. 10a), the lowest radar beam slopes upward over the descending terrain. Using the KICX mountaintop VCP (Fig. 10b), the lowest elevation angle slopes downward then upward, remaining within 1–2 km of the sloping terrain. Storms that are overshot using VCP 11 easily would be detected using the mountaintop VCP.

6. Composite radar coverage

The advantages of using mountaintop VCPs across the entire three-radar coverage area are illustrated in Fig. 11 in terms of the terrain-relative heights of the lowest unblocked beams. Much of the terrain within 100–150 km of the three radars, and some of it out to 230 km, lies within 1 km of the lowest unblocked beam (about 30% of the coverage area). Along the heavily populated corridor from Ogden to Provo in Utah, the coverage is 100%. In contrast, the centers of the beams from the three radars using VCP 11 (Fig. 1b) are within 1 km of the ground for only 2% of the overall coverage area.

With the marked increase in areal coverage using negative elevation angles, forecasters could do a much better job of detecting the presence of, and following the evolution of, a variety of lower-altitude weather events that currently are partially or totally undetectable. These weather events include frontal and outflow boundaries that trigger new convection, strong wind events such as microbursts, and the occurrence of mesocyclone and tornadic vortex signatures at low and midaltitudes in distant storms. Especially important would be the ability to detect and more accurately estimate heavy rainfall and snowfall accumulations on the ground.

7. Summary and conclusions

National Weather Service forecasters rely heavily on WSR-88D measurements for the issuance of severe weather warnings and quantitative precipitation estimates (QPEs). In the western United States, about one-third of these radars are located on the tops of mountains where they potentially could provide good coverage of hazardous weather events that affect the populace at lower altitudes. Unfortunately, the NWS currently does not allow its forecasters to scan their radars at lower elevation angles where many of the hazardous events can be best detected. The policy is for all WSR-88Ds—both flatland and mountaintop—to use +0.5° as the lowest elevation angle. This means that mountaintop radars frequently fail to detect or to adequately diagnose the presence of hazardous weather phenomena.

As far as WSR-88D coverage is concerned, the state of Utah is especially disadvantaged because all three of the radars that cover the state are on the tops of mountains. In order to estimate what could be gained by scanning at lower elevation angles, we used a simulation model to produce scanning strategies that include negative elevation angles. The simulation model did not

consider practical operational problems that could arise owing to radar beam sidelobes, increased ground clutter, or anomalous propagation caused by nonstandard conditions for the index of refraction.

Based on the results in this study, we determined a reasonable lowest elevation angle for the KMTX radar near Salt Lake City to be −0.4°, and for KICX near Cedar City and KGJX near Grand Junction to both be −0.9°. To aid in the far-range detection of hazardous weather, the lowest several elevation angles were separated by 0.4°–0.5° instead of the customary 1°.

The WSR-88D system contains numerous algorithms that use Doppler radar base data as input to produce meteorological and hydrological products (Crum and Alberty 1993). WSR-88D datasets collected using experimental mountaintop VCPs should be used to test and evaluate algorithm performance to ensure that the algorithms function properly.

The results of the simulations discussed in this paper are encouraging. Though the lower elevation angles of the mountaintop VCP experience more blockage than the elevation angles of the current VCPs, there is a marked increase in the ability to detect what is taking place within 1 km of the ground. Using the conventional scanning strategies with their upward-pointing elevation angles, the lowest unblocked elevation angle is within 1 km of the terrain for only 2% of the area covered by the three radars. However, using negative elevation angles, the lowest unblocked elevation angle is within 1 km of the terrain for over 30% of the area. In fact, along the heavily populated corridor between Odgen and Provo, the coverage within 1 km of the ground is 100% for the mountaintop VCP. It is within the lowest 1 km where the best estimates of rainfall and snowfall accumulations are made, where strong outflow winds occur, and where the boundaries that initiate convection occur. Without having these types of information available, forecasters are at an undue disadvantage as they try to warn the public of impending dangers.

Acknowledgments. We appreciate the comments of Larry Dunn and Dave Sanders of the Salt Lake City NWS Forecast Office and of Mike Meyers and Jeff Colton of the Grand Junction NWS Forecast Office, who related the types of weather phenomena that they fail to detect or resolve owing to the current WSR-88D scanning strategies. David Schultz (NSSL), J. J. Gourley (NSSL), and two anonymous reviewers provided helpful comments and suggestions on this manuscript. The expertise and advice of Dale Sirmans, RS Information Systems, were essential during the development of the simulated scanning strategies. This research was funded by the National Severe Storms Laboratory.

REFERENCES

Battan, L. J., 1973: *Radar Observations of the Atmosphere.* 3d ed. The University of Chicago Press, 324 pp.

Brown, R. A., V. T. Wood, and D. Sirmans, 2000: Improved WSR-88D scanning strategies for convective storms. *Wea. Forecasting,* **15,** 208–220.

——, ——, and T. W. Barker, 2002: Improved detection using negative elevation angles for mountaintop WSR-88Ds: Simulation of KMSX near Missoula, Montana. *Wea. Forecasting,* **17,** 223–237.

Carpenter, D. M., 1993: The lake effect of the Great Salt Lake: Overview and forecast problems. *Wea. Forecasting,* **8,** 181–193.

Colton, J. D., C. N. Jones, and M. P. Meyers, 2000: A rare tornadic thunderstorm in northeast Utah. Preprints, *Ninth Conf. on Mountain Meteorology,* Aspen, CO, Amer. Meteor. Soc., 186–189.

Crum, T. D., and R. L. Alberty, 1993: The WSR-88D and the WSR-88D Operational Support Facility. *Bull. Amer. Meteor. Soc.,* **74,** 1669–1687.

——, ——, and D. W. Burgess, 1993: Recording, archiving, and using WSR-88D data. *Bull. Amer. Meteor. Soc.,* **74,** 645–653.

Davis, R. S., and P. Jendrowski, 1996: The operational Areal Mean Basin Estimated Rainfall (AMBER) module. Preprints, *15th Conf. on Weather Analysis and Forecasting,* Norfolk, VA, Amer. Meteor. Soc., 332–335.

Doviak, R. J., and D. S. Zrnić, 1993: *Doppler Radar and Weather Observations.* 2d ed. Academic Press, 562 pp.

Dunn, L. B., and S. V. Vasiloff, 2001: Tornadogenesis and operational considerations of the 11 August 1999 Salt Lake City tornado as seen from two different Doppler radars. *Wea. Forecasting,* **16,** 377–398.

Filiaggi, M. T., S. B. Smith, M. Churma, L. Xin, and M. Glaudemans, 2002: Flash Flood Monitoring and Prediction version 2.0: Continued AWIPS modernization. Preprints, *Interactive Symp. on the Advanced Weather Interactive Processing System* (*AWIPS*), Orlando, FL, Amer. Meteor. Soc, J179–J182.

Fulton, R. A., J. P. Breidenbach, D.-J. Seo, D. A. Miller, and T. O'Bannon, 1998: The WSR-88D rainfall algorithm. *Wea. Forecasting,* **13,** 377–395.

Maddox, R. A., J. Zhang, J. J. Gourley, and K. W. Howard, 2002: Weather radar coverage over the contiguous United States. *Wea. Forecasting,* **17,** 927–934.

National Weather Service, 2000: Pedestal System Operations and Maintenance Instructions. NWS Tech. Manual EHB 6-514, xxii + 297 pp. [Available from WSR-88D Radar Operations Center, 1200 Westheimer Dr., Norman, OK 73069.]

Smith, P. L., 1998: On the minimum useful elevation angle for weather surveillance radar scans. *J. Atmos. Oceanic Technol.,* **15,** 841–843.

Steenburgh, W. J., S. F. Halvorson, and D. J. Onton, 2000: Climatology of lake-effect snowstorms of the Great Salt Lake. *Mon. Wea. Rev.,* **128,** 709–727.

SRI International, 1993: Final supplemental environmental assessment (SEA) of the effects of electromagnetic radiation from the WSR-88D radar. Report for the Next Generation Weather Radar Joint System Program Office, 498 pp. [Available from WSR-88D Radar Operations Center, 1200 Westheimer Dr., Norman, OK 73069.]

Vasiloff, S. V., 2001: Improving tornado warnings with the Federal Aviation Administration's terminal Doppler weather radar. *Bull. Amer. Meteor. Soc.,* **82,** 861–874.

Wilson, J. W., and W. E. Schreiber, 1986: Initiation of convective storms by radar-observed boundary layer convergent lines. *Mon. Wea. Rev.,* **114,** 2516–1536.

——, and C. K. Mueller, 1993: Nowcasts of thunderstorm initiation and evolution. *Wea. Forecasting,* **8,** 113–131.